Impacts of $PM_{2.5}$ Chemical Composition on Aerosol Light Extinction During the Xi'an International Horticultural Expo of China

Qiyuan Wang[1,2,*], Yaqing Zhou[3], Suixin Liu[1,2], Ting Zhang[1,2] and Jie Tian[1,2]

[1]*Key Laboratory of Aerosol Chemistry and Physics (KLACP) and State Key Laboratory of Loess and Quaternary Geology (SKLLQG), Institute of Earth Environment, Chinese Academy of Sciences, Xi'an 710061, China*

[2]*CAS Center for Excellence in Quaternary Science and Global Change, Xi'an 710061, China*

[3]*Institute for Environmental and Climate Research, Jinan University, Guangzhou 511443, China*

Abstract: In this study, we investigated the impacts of $PM_{2.5}$ chemical composition on aerosol light extinction during the Xi'an International Horticultural Expo of China. The average mass concentration of $PM_{2.5}$ was 118.1 ± 57.3 μg m^{-3} during the entire campaign with 23.1% and 40.7% contributed by carbonaceous aerosols and water-soluble inorganic ions. The average light extinction was 957.7 ± 643.5 Mm^{-1}, of which >90% was contributed by the particle light scattering. The light extinction was 1.6 times larger during polluted period than the unpolluted period. The diurnal pattern of the measured light scattering was associated with the anthropogenic activities of daily life and the daily variation of boundary-layer height. Based on the IMPROVE equation, $(NH_4)_2SO_4$ was the largest contributor to light extinction (35.3%) during the Xi'an International Horticultural Expo, followed by organic matter (33.7%), NH_4NO_3 (20.5%), EC (6.3%), and fine soil (4.0%). The light extinction produced by $(NH_4)_2SO_4$, organic matter, and NH_4NO_3 were 1.8 – 2.5 times larger during polluted period than the unpolluted period. The results indicated that $(NH_4)_2SO_4$ was the most important chemical composition in $PM_{2.5}$ affecting the aerosol light extinction during the Xi'an International Horticultural Expo.

Keywords: Light extinction, $PM_{2.5}$, Chemical composition, Air pollution.

1. INTRODUCTION

Atmospheric aerosols have been gaining substantial attention due to their important impacts on global energy budget and climate [1-3]. Aerosols can perturb the Earth's radiation balance directly causing either cooling or heating of the atmosphere through scattering and absorbing solar radiation [4]. It can also indirectly affect by changing the microphysical properties of clouds [5]. Furthermore, previous studies have been demonstrated that aerosols can be inhaled deep into the lungs, and thus can cause a great threat to human health [6, 7]. It has been reported that atmospheric aerosols can also alter surface air temperature, precipitation, and have adverse effects on visibility reduction in urban and regional areas [8-12].

The radiative effects and visibility degradation are related to the aerosol optical properties, especially the light extinction (b_{ext}, including light scattering and absorption) [8, 12]. Due to the inconsistency of aerosol concentrations and its composition in spatial and temporal distribution, there are still large uncertainties in determining the impacts of aerosol on particle's optical properties. To reduce the uncertainties, more assessment of relationships between aerosol optical properties and aerosol chemical composition, microphysical properties, and probable sources is required at local, regional, even global scales.

In recent years, with the development of urbanization, Chinese cities are facing severe air pollution [13]. High loading of fine particulate matter ($PM_{2.5}$ with aerodynamic diameter ≤2.5 μm) is a main cause of the air pollution, especially during winter [14]. Several studies in China have investigated the relationship between the $PM_{2.5}$ chemical composition and particle's light extinction under different atmospheric environment [15-22]. For example, Wang *et al*. [18] reported that the b_{ext} in Chengdu (a megacity in southwest of China) was mainly contributed by $(NH_4)_2SO_4$ and NH_4NO_3. In contrast, Wang *et al*. [19] found that organic matter (OM), rather than inorganic aerosol, was the largest contributor (54%) to particle light scattering during winter in Beijing. In addition, Deng *et al*. [15] showed that sea salt was an important contributor to b_{ext} (14%) in a coastal city of China. The previous studies also indicate that the relationship between the chemical species and b_{ext} is strongly associated with both geographically and temporally.

*Address correspondence to this author at the Key Laboratory of Aerosol Chemistry and Physics (KLACP) and State Key Laboratory of Loess and Quaternary Geology (SKLLQG), Institute of Earth Environment, Chinese Academy of Sciences, Xi'an 710061, China; Tel: +86-029-62336272;
E-mail: wangqy@ieecas.cn

E-ISSN: 2311-8741/20

Guanzhong Basin is one of the largest basins in China. Several investigations have shown that the Guanzhong Basin suffers from huge loadings of $PM_{2.5}$, especially in wintertime [23-25]. Xi'an is located on the Guanzhong Basin at the southern edge of the Loess Plateau, which has a resident population of >10 million. Although the local government in Xi'an has adopted some air pollutant control measures, the annual $PM_{2.5}$ mass concentration is still very high. The large loadings of $PM_{2.5}$ can affect air quality and atmospheric visibility. To improve the living environment of the residents, it is necessary to understand the effects of different chemical components on particle extinction. Therefore, the main objectives of this study were (1) to investigate the characteristics of b_{ext} and $PM_{2.5}$ chemical components and (2) to determine the contributions of $PM_{2.5}$ chemical composition to b_{ext}.

2. EXPERIMENTAL

2.1. Sampling and Analytical Methods

An intensive measurement was conducted at an urban-scale site of Xi'an, China on the rooftop (10 m above ground level) of the Institute of Earth Environment, Chinese Academy of Science (34.23 °N, 108.88 °E) (Figure **1**). This site is ~15 km southwest of downtown Xi'an, and it is surrounded by a residential/commercial area. The sampling period was during the Xi'an International Horticultural Expo (XA-IHE) from 28 April to 22 October 2011. The entire campaign was divided into three seasons, that is, April to May for spring, June to August for summer, and September to October for autumn.

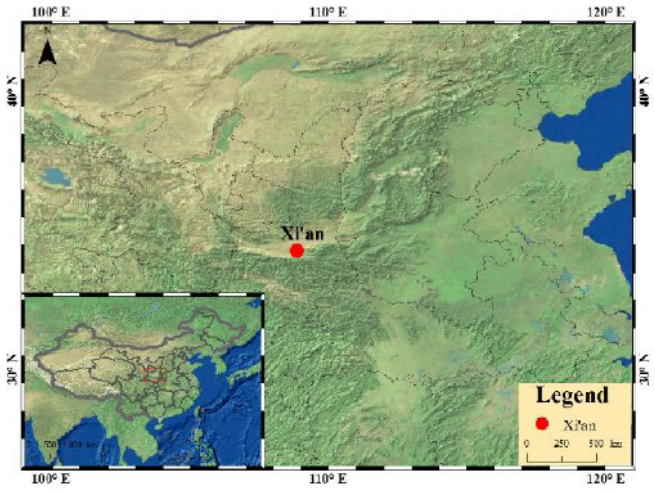

Figure 1: Map showing the Xi'an sampling site and surrounding areas. The map was drawn using ArcGIS software. The base map is the World Topographic Map from ESRI (www.arcgis.com/home/item.html?id=30e5fe3149c34df1ba922e6f5bbf808f).

Daily $PM_{2.5}$ samples were collected using two battery-powered mini-volume samplers (Airmetrics, Oregon, USA) with an operating flow rate of 5 L min^{-1}. One was collected onto 47 mm Whatman quartz microfiber filters (QM/A; Whatman, Middlesex, UK) for water-soluble ions and carbonaceous analyses; the other was collected onto 47 mm Teflon filters (Whatman Limited, Maidstone, UK) for inorganic elemental analyses. Each sample was collected for 24 h from 10:00 am to 10:00 am the next day. The quartz filters were preheated to 800 °C for 3 h before sampling. The filters were equilibrated in a box with controlled relative humidity (RH: 35–45%) and temperature (20–23 °C). After 24 h later, the filters were then weighed on a Sartorius MC5 electronic microbalance with a ±1 μg sensitivity (Sartorius, GÖttingen, Germany). After sampling, the filters were stored in a refrigerator at about 4 °C before chemical analysis. Field blank filters were collected to subtract the positive artifacts due to adsorption of gas-phase organic components onto the filter during and/or after sampling.

An ion chromatography (IC, Dionex 600, Dionex Corp, Sunnyvale, CA) was used to determine water-soluble inorganic ions [26]. Cations (*i.e.*, K^+, Mg^{2+}, Ca^{2+}, and NH_4^+) were analyzed with a CS12A column (Dionex Company) with 20 mM methanesulfonic acid eluent. Anions (*i.e.*, F^-, Cl^-, SO_4^{2-}, NO_3^-) were separated by an ASII-HC column (Dionex Company) with the use of 20 mM potassium hydroxide as the eluent. The detection limits for anions and cations were less than 0.05 mg L^{-1}. Standard Reference Materials produced by the National Research Center for Certified Reference Materials in China were analyzed for quality assurance and quality control purposes. Blank values were subtracted from the sample concentrations.

A DRI Model 2001 Thermal/Optical Carbon Analyzer (Atmoslytic Inc., Calabasa, CA, USA) was used to analyze the carbonaceous species, including organic carbon (OC) and element carbon (EC) [27]. The method produced data for four OC fractions (including OC1, OC2, OC3, and OC4 in a helium atmosphere at 140 °C, 280 °C, 480 °C, and 580 °C, respectively), a pyrolyzed carbon fraction (OP, determined when reflected laser light attained its original intensity after oxygen was added to the combustion atmosphere), and three EC fractions (including EC1, EC2, and EC3 in a 2% oxygen/ 98% helium atmosphere at 580 °C, 740 °C, and 840 °C, respectively). The IMPROVE_A protocol defines OC as OC1 + OC2 + OC3 + OC4 + OP and EC as EC1 + EC2 + EC3 - OP. The analyzer was calibrated daily with

known quantities of CH_4. Replicate analyses were performed at a rate of one per group of ten samples. Field blank samples were also analyzed, and the sample results were corrected by the blank sample concentration. More detailed descriptions of the Quality Assurance/Quality Control procedures can be found in Cao *et al*. [28].

An Energy Dispersive X-Ray Fluorescence (ED-XRF) spectrometry (Epsilon 5 ED-XRF, PANalytical B.V., The Netherlands) was used to determine the inorganic elements [29]. The ED-XRF uses a three-dimensional polarizing geometry with 11 secondary targets (*e.g*., CeO_2, CsI, Ag, Mo, Zr, KBr, Ge, Zn, Fe, Ti, and Al) and one barkla target (Al_2O_3) that supplies a good signal to the background ratio, providing the low detection limits. The X ray source is a side window X ray tube with a Gadolinium (Gd) anode, which is operated at an accelerating voltage of 25–100 kV and a current of 0.5–24 mA (maximum power: 600 W). The X-ray characteristic radiation is detected by a Germanium (Ge) detector (PAN 32). Each sample was analyzed for half an hour and filed blank of Teflon filter sample was analyzed to evaluate analytical bias. The elements that determined by the ED-XRF method were S, Cl, K, Ca, Ti, Mn, Fe, Ni, Zn, As, Br, and Pb.

An Ecotech Aurora-1000 single wavelength integrating nephelometer (Melbourne, Australia) was used to measure the light scattering coefficient. The nephelometer determines particle light scattering coefficient continuously at a wavelength of 520 nm. Span calibration was carried out every week with R-134 gas, while zero calibration was performed every two days with particle-free air to subtract the Rayleigh scattering component from the light scattering coefficient. The nephelometer drew the ambient air through a temperature-controlled inlet at a flow rate of 5 L min^{-1}. The processor-controlled heating system automatically maintained the RH in the chamber below 60%. The time-resolution of light scattering coefficient was 5 min.

Nitrogen dioxide (NO_2) was measured by a Nitrogen Oxides Analyzer (Ecotech EC9841, Melbourne, Australia). The detection of NO_2 was 0.5 ppb. The relative humidity (RH) was obtained from Shaanxi Provincial Meteorological Bureau, which is ~25 km north from the sampling site.

2.2. Data Analysis

The total light extinction coefficient (b_{ext}) constitutes two parts: one is the aerosol light scattering and absorption (b_{sp} and b_{ap}), and the other is the light scattering and absorption caused by gases (b_{sg} and b_{ag}) [30]. Thus, the b_{ext} can be estimated as follows:

$$b_e = b_s + b_a + b_s + b_a \quad (1)$$

The b_{sp} has long been known to be influenced by relative humidity [31]. Thus, a relative correction factor was applied to compensate for the effect of RH when yielding the dry b_{sp} as follows [32]:

$$b_{s,w} = f(RH) \times b_{s,d} \quad (2)$$

where $b_{sp,wet}$ is the light scattering coefficient considering atmospheric RH; f(RH) denotes the scattering enhancement factor affected by RH; and $b_{sp,dry}$ is the dry scattering coefficient measured by the nephelometer. The f(RH) curve that from Malm *et al*. [32] for estimating the effect of humidity on aerosol b_{sp} was employed in this study.

The b_{ap} at wavelength of 520 nm is mainly produced by black carbon in the atmosphere [33]. Since there was no measured b_{ap}, it was estimated using the formula below [34]:

$$b_a = 10 \times [EC] \quad (3)$$

where [EC] denotes the mass concentration of EC (μg m^{-3}) and the factor of 10 denotes the mass absorption cross section of EC (m^2 g^{-1}). The b_{ag} is mainly contributed by NO_2 gas, which was estimated as follows [34]:

$$b_a = 0.33 \times [NO_2] \quad (4)$$

where the [NO_2] is the NO_2 mixing ratio in ppb and the factor of 0.33 describes the absorption efficiency of NO_2 (Mm^{-1} ppb^{-1}). The b_{sg} is caused by Rayleigh scattering, which was assumed to be a constant of 10 Mm^{-1} [30].

To establish the relationship between the aerosol optical properties and its chemical species, the revised IMPROVE equation was used to estimate the b_{ext} contributed by $PM_{2.5}$ chemical composition. The revised IMPROVE algorithm is as follows [34]:

$$b_e \approx 2.2 \times f_s(R) \times [S \quad S \quad] + 4.8 \times f_L(R) \times [L \quad S \quad] + 2.4 \times f_s(R) \times [S \quad N \quad] + 5.1 \times f_L(R) \times [L \quad N \quad] + 2.8 \times [S \quad O \quad M \quad] + 6.1 \times [L \quad O \quad M \quad] + 10 \times [E \quad C \quad] + 1 \times [F \quad S \quad] + 1.7 \times f_s(R) \times [S \quad S \quad] + 0.6 \times [C \quad M \quad] + R \quad hS \quad + 0.33 \times [N_2] \quad (5)$$

The apportionment of the mass concentrations of

small and large sulfate/nitrate/organic mass is defined by IMPROVE equation as follows:

$$[\text{Large X}] = \frac{[\text{T} \quad \text{X}]^2}{2}, \text{for } [\text{Total X}] < 20\ \mu \quad \text{m}^{-3} \tag{6}$$

$$[Large\ X] = [Total\ X], for [Total\ X] \geq 20\ \mu g\ m^{-3} \tag{7}$$

$$[Small\ X] = [Total\ X] - [Large\ X] \tag{8}$$

where X denotes the sulfate, nitrate, or organic matter. The sulfate and nitrate were assumed to $(NH_4)_2SO_4$ and NH_4NO_3, respectively, and their mass concentrations were calculated by multiplying the concentrations of SO_4^{2-} and NO_3^- by factors of 1.375 and 1.29, respectively. The mass concentration of organic matter (OM) was estimated by multiplying the amount of OC by 1.60 [35]. The concentration of fine soil was calculated by Fe as follows [36]:

$$[\text{Fine Soil}] = \left(\frac{1}{0.0}\right) \times [\text{Fe}] \tag{9}$$

3. RESULTS AND DISCUSSION

3.1. $PM_{2.5}$ and its Chemical Composition

Table **1** summarizes the seasonal variations of $PM_{2.5}$ mass concentration during the XA-IHE period. The daily $PM_{2.5}$ mass concentration ranged from 23.0 – 318.9 μg m^{-3} with an average value of 118.1 ± 57.3 μg m^{-3} during the entire campaign. The average $PM_{2.5}$ loading exceeded the Grade II of Chinese National Ambient Air Quality Standards (NAAQS) of daily mass concentration of $PM_{2.5}$ (75 μg m^{-3}, GB3095-2102) by a factor of 1.6. During the 178 days of XA-IHE, only 41 days (23%) reached the Grade II of NAAQS, indicating a serious air pollution in Xi'an. For different seasons, the $PM_{2.5}$ mass concentration was the highest in spring (129.6 ± 68.5 μg m^{-3}), followed by autumn (122.1 ± 65.1 μg m^{-3}) and summer (112.0 ± 47.5 μg m^{-3}).

The mass concentrations of OC and EC were 21.3 μg m^{-3} and 4.6 μg m^{-3} during the XA-IHE period, accounting for 19.2% and 3.9% of $PM_{2.5}$ mass, respectively. The seasonal variations of OC and EC contributions to $PM_{2.5}$ both exhibited autumn > summer > spring. Figure **2** shows that the correlation between OC and EC was good in spring (r = 0.71) and autumn (r = 0.90), indicating that primary emission was an important source for OC. However, weak correlation was found for OC and EC in summer, indicating that secondary formation may be important for OC. The mass concentration of water-soluble inorganic ions was 31.2 μg m^{-3}, accounting for 40.7% of $PM_{2.5}$ during the XA-IHE. Among the ions, the secondary water-soluble inorganic ions (*i.e.*, SO_4^{2-}, NO_3^-, and NH_4^+) contributed 82.0% of total ions. The cations ranked in the order of $NH_4^+ > Na^+ > Ca^{2+} > K^+ > Mg^{2+}$, and the anions exhibited the order of $SO_4^{2-} > NO_3^- > Cl^- > F^-$. For the elements, S, Ca, Zn, K, Cl, and Fe were abundant, which together accounted for 80% of total elements.

3.2. Aerosol Optical Properties

Table **2** summarizes the seasonal variations of aerosol optical properties during the XA-IHE period. The average b_{ext} was 957.7 ± 643.5 Mm^{-1} during the campaign, with the largest in autumn (1144.1 Mm^{-1}), followed by summer (920.6 Mm^{-1}) and spring (608.5 Mm^{-1}). The average $b_{sp,wet}$ was 920.6 ± 625.4 Mm^{-1} with the highest in autumn (1077.4 Mm^{-1}), followed by

Table 1: **Summary of the Mass Concentration of $PM_{2.5}$ and its Chemical Species During the Campaign (unit: μg m^{-3})**

Species	Spring	Summer	Autumn	All data
$PM_{2.5}$	129.6	112	122.1	118.1
OC	18.4	19.2	25.2	21.3
EC	3.1	4.1	5.6	4.6
Na^+	2.1	2.5	1.9	2.2
NH_4^+	2.7	7.8	8.9	7.4
K^+	0.6	0.9	1.2	1
Mg^{2+}	0.7	0.7	0.3	0.6
Ca^{2+}	4.1	0.7	0	1.6
F^-	0.7	0.6	0.4	0.5
Cl^-	3.2	3	3.3	3.1
NO_3^-	8	10.5	19.1	12.7
SO_4^{2-}	10.7	23.7	20.9	20.8

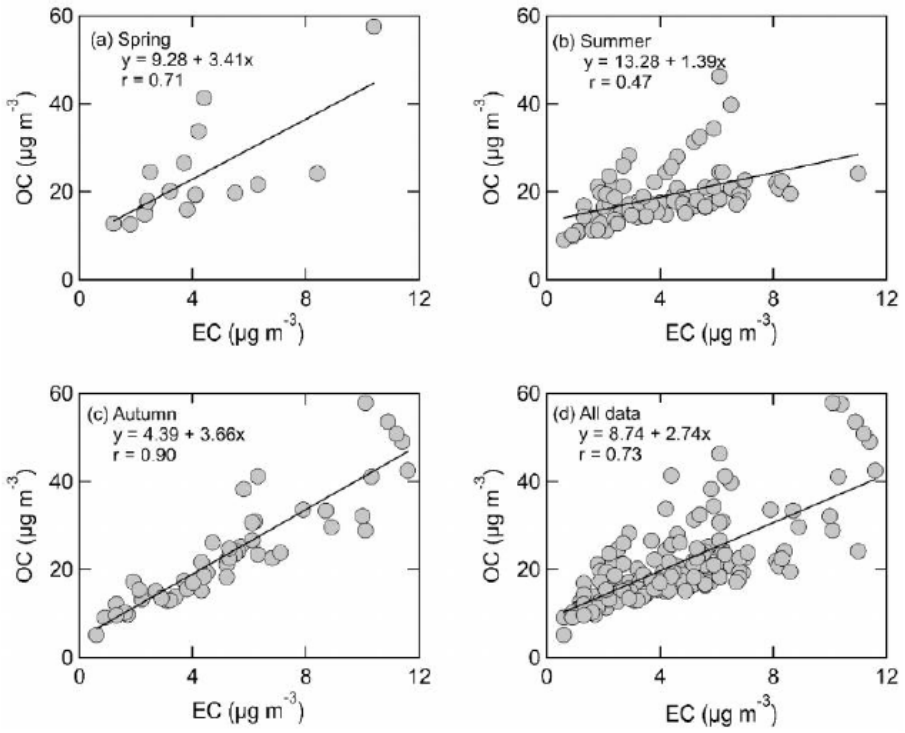

Figure 2: Scatter plots of organic carbon (OC) versus elemental carbon (EC) during (**a**) spring, (**b**) summer, (**c**) autumn, and (**d**) the entire campaign period.

summer (898.5 Mm^{-1}) and spring (576.7 Mm^{-1}). The average b_{abs} was 42.8 ± 26.9 Mm^{-1} with the largest in autumn (52.5 ± 31.3 Mm^{-1}), followed by summer (39.5 ± 22.4 Mm^{-1}) and spring (32.9 ± 26.5 Mm^{-1}). The $b_{sp,wet}$ accounted for >90% of b_{ext} during different seasons, indicating the light scattering particle was the dominant contributor to aerosol optical properties. Table **2** also summarizes the aerosol optical properties under polluted and unpolluted periods. The b_{ext} during polluted period (1006.5 ± 652.8 Mm^{-1}) was 1.6 times larger than the unpolluted period (611.9 ± 505.5 Mm^{-1}). Both light scattering and absorption coefficients presented higher values for polluted period compared with the unpolluted period, and this is consistent with the variation of $PM_{2.5}$ loading.

Table 2: **Summary of the Light Extinction and Light Absorption During Different Periods**

Period	Light extinction (Mm^{-1})	Light absorption (Mm^{-1})
Spring	608.5	32.9
Summer	920.6	39.5
Autumn	1144.1	52.5
Polluted period	1006.5	41.9
Unpolluted period	611.9	36.5
All data	957.7	42.8

Diurnal variations of $b_{sp,dry}$ in different seasons (Figure **3**) were used to reflect the impact of particulate matter on b_{ext}. As shown in Figure **3a**, the $b_{sp,dry}$ exhibited a pattern of "two peaks and two valleys" during spring. The lowest $b_{sp,dry}$ (249.1 Mm^{-1}) was observed in the afternoon of 17:00; and it increased gradually until 03:00 reaching the highest value of 474.8 Mm^{-1}; after then, $b_{sp,dry}$ decreased reaching the lowest value of 371.7 Mm^{-1} in the early morning of 06:00; then the $b_{sp,dry}$ increased again and reached to the peak of 427.0 Mm^{-1} at 09:00. Different from the variation in spring, the $b_{sp,dry}$ in summer shows a single peak change characteristics with the highest value observed at 05:00 (636.5 Mm^{-1}). The $b_{sp,dry}$ then decreased to the low value of 454.4 Mm^{-1} at 17:00, and then increased gradually at night. During autumn, a continuous peak was found in the morning of 08:00–12:00; after then $b_{sp,dry}$ decreased to the minimum value of 489.4 Mm^{-1} at 18:00, and then increased to the maximum value of 621.8 Mm^{-1} at midnight. Although the diurnal patterns of $b_{sp,dry}$ varied with seasons, they mainly controlled by the anthropogenic activity pattern of daily life and the daily variation in boundary-layer height. The peak in the morning was mainly attributed to the rush-hour traffic while the enhancement at night was due to the enhanced anthropogenic activities (*e.g.*, rush-hour traffic and cooking) combined with the low boundary-layer height which promoted to accumulate

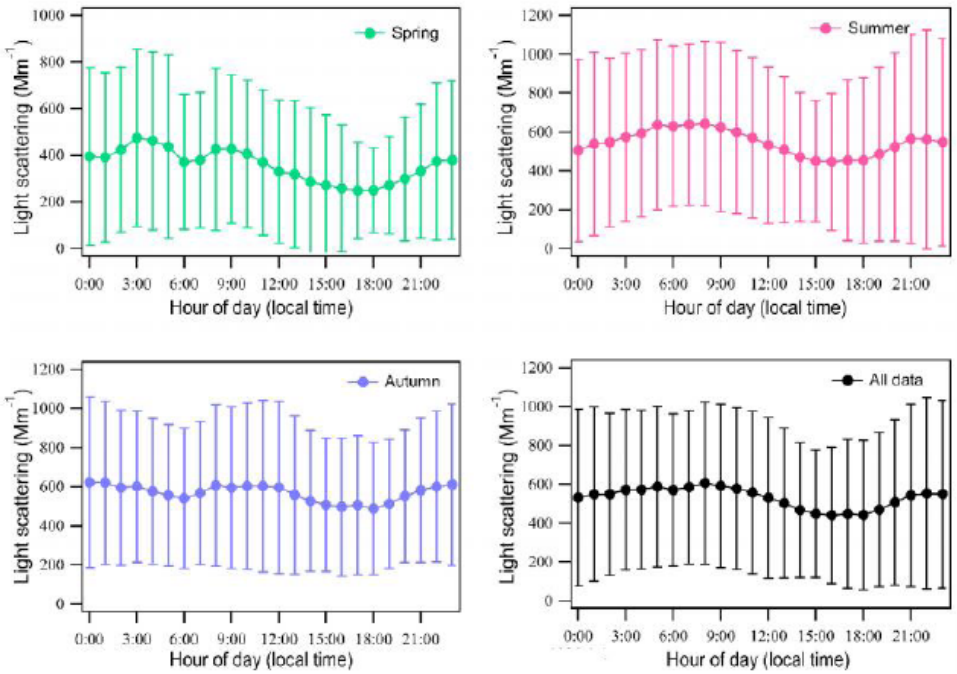

Figure 3: Diurnal variations of particle light scattering during different seasons and entire campaign period.

the pollutants. The low valley in the afternoon was associated with the enhanced boundary-layer height which led to dilution of the particulate matter and as a result lower $b_{sp,dry}$ in the afternoon.

3.3. Impacts of $PM_{2.5}$ and its Chemical Composition on b_{ext}

Table **3**-**5** show correlations between $b_{sp,dry}$ and $PM_{2.5}$ as well as its chemical components. The $b_{sp,dry}$ showed stronger correlations with $PM_{2.5}$ mass concentration during spring (r = 0.73) and autumn (r = 0.84) compared with the summer (r = 0.65), indicating that there may be other factors influencing the $b_{sp,dry}$ in addition to $PM_{2.5}$. Among chemical species, secondary water-soluble inorganic ions (*i.e.*, SO_4^{2-}, NO_3^-, and NH_4^+) showed well correlations with $b_{sp,dry}$ during three seasons, indicating that those ions were important contributors to aerosol optical properties. Furthermore, the $b_{sp,dry}$ correlated strongly with K^+ in spring and autumn but had weak correlation in summer, indicating

Table 3: **Correlation Among Light Scattering (b_{sp}), $PM_{2.5}$ Mass, and Chemical Components During Spring**

Parameter	b_{sp}	$PM_{2.5}$	SO_4^{2-}	NO_3^-	F^-	Cl^-	NH_4^+	Na^+	K^+	Mg^{2+}	OC	EC
b_{sp}	1.00											
$PM_{2.5}$	0.73	1.00										
SO_4^{2-}	0.84	0.63	1.00									
NO_3^-	0.68	0.15	0.79	1.00								
F^-	-0.13	0.12	-0.06	-0.05	1.00							
Cl^-	0.37	0.17	0.03	0.25	0.41	1.00						
NH_4^+	0.76	0.23	0.84	0.96	-0.25	0.18	1.00					
Na^+	0.35	0.10	0.51	0.63	0.49	0.46	0.51	1.00				
K^+	0.66	0.57	0.74	0.44	0.01	0.17	0.51	0.38	1.00			
Mg^{2+}	0.45	0.81	0.39	0.03	0.59	0.26	-0.02	0.23	0.38	1.00		
OC	0.86	0.88	0.61	0.25	0.06	0.38	0.34	0.20	0.65	0.69	1.00	
EC	0.41	0.43	0.02	-0.15	-0.29	0.46	0.02	-0.25	0.17	0.09	0.54	1.00

Table 4: Correlation Among Light Scattering (b_{sp}), $PM_{2.5}$ Mass, and Chemical Components During Summer

Parameter	b_{sp}	$PM_{2.5}$	SO_4^{2-}	NO_3^-	F^-	Cl^-	NH_4^+	Na^+	K^+	Mg^{2+}	OC	EC
b_{sp}	1.00											
$PM_{2.5}$	0.65	1.00										
SO_4^{2-}	0.70	0.81	1.00									
NO_3^-	0.72	0.66	0.66	1.00								
F^-	-0.04	0.10	0.05	0.05	1.00							
Cl^-	0.13	0.23	0.06	0.33	0.74	1.00						
NH_4^+	0.80	0.82	0.96	0.82	-0.01	0.11	1.00					
Na^+	0.35	0.42	0.53	0.49	0.52	0.56	0.49	1.00				
K^+	0.41	0.60	0.57	0.41	0.00	0.14	0.55	0.36	1.00			
Mg^{2+}	0.06	0.16	0.07	0.09	0.94	0.76	0.02	0.54	0.01	1.00		
OC	0.23	0.45	0.29	0.23	0.59	0.57	0.25	0.36	0.42	0.60	1.00	
EC	0.55	0.78	0.71	0.67	0.09	0.28	0.73	0.44	0.47	0.15	0.41	1.00

Table 5: Correlation Among Light Scattering (b_{sp}), $PM_{2.5}$ Mass, and Chemical Components During Autumn

Parameter	b_{sp}	$PM_{2.5}$	SO_4^{2-}	NO_3^-	F^-	Cl^-	NH_4^+	Na^+	K^+	Mg^{2+}	OC	EC
b_{sp}	1.00											
$PM_{2.5}$	0.84	1.00										
SO_4^{2-}	0.94	0.81	1.00									
NO_3^-	0.80	0.90	0.76	1.00								
F^-	0.19	0.51	0.22	0.27	1.00							
Cl^-	0.15	0.51	0.08	0.29	0.51	1.00						
NH_4^+	0.93	0.91	0.93	0.93	0.24	0.20	1.00					
Na^+	0.05	0.28	0.06	0.09	0.27	0.85	0.07	1.00				
K^+	0.84	0.94	0.82	0.91	0.39	0.36	0.91	0.18	1.00			
Mg^{2+}	0.58	0.66	0.58	0.49	0.61	0.40	0.54	0.23	0.59	1.00		
OC	0.57	0.87	0.52	0.74	0.61	0.54	0.66	0.23	0.80	0.58	1.00	
EC	0.56	0.79	0.47	0.60	0.62	0.55	0.55	0.27	0.73	0.67	0.91	1.00

that the aerosol optical properties were influenced by biomass burning in spring and autumn.

Figure **4** shows the results of the reconstructed b_{ext} by IMPROVE equation and the measured b_{ext} with nephelometer. The reconstructed b_{ext} correlated strongly with the measured values during spring, summer, and autumn with correlation coefficients of 0.87, 0.94, and 0.85, respectively, indicating that there is a good consistency between them. The slope which reflects differences in absolute values between the reconstructed and measured b_{ext} was 0.94 for spring, 0.48 for summer, and 0.71 for autumn. Therefore, the reconstructed results were reasonable for spring and autumn, however, the low slope for summer may be due to the various mass absorption efficiencies of chemical species in different areas. Moreover, because the nephelometer measured the light scattering of total suspended particulate, but the IMPROVE equation is based on the $PM_{2.5}$ chemical composition which therefore made an underestimated result.

Figure **5** shows the contributions of $PM_{2.5}$ chemical composition to b_{ext} based on the results of IMPROVE equation. From the entire XA-IHE period, $(NH_4)_2SO_4$ was the largest contributor to b_{ext}, and its b_{ext} was 272.2 Mm^{-1} accounting for 35.3% of total b_{ext}. OM was the second largest contributor to b_{ext} (204.6 Mm^{-1}, 33.7%), followed by NH_4NO_3 (168.4 Mm^{-1}, 20.5%), EC (42.8 Mm^{-1}, 6.3%), fine soil (23.6 Mm^{-1}, 4.0%), and NO_2

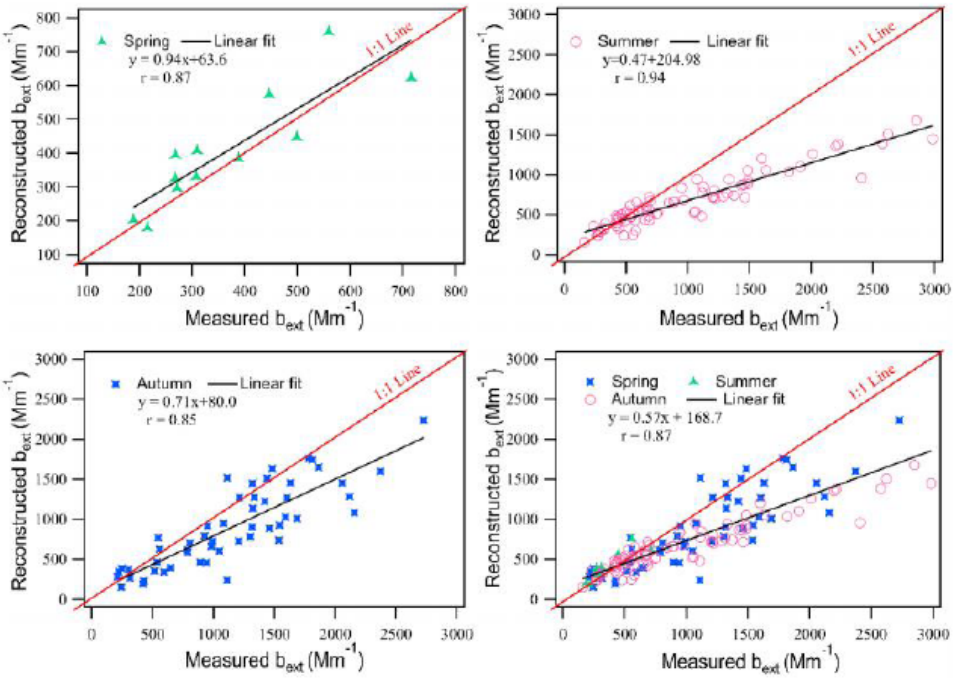

Figure 4: Scatter plots of reconstructed particle light extinction (b_{ext}) versus measured ones during different seasons and entire campaign period.

(3.9 Mm^{-1}, 0.7%). From the seasonal perspective, the contributions of $PM_{2.5}$ chemical species were different. For spring, the b_{ext} produced by OM was 211.2 Mm^{-1} accounting for 48.5% of b_{ext}, which was the largest contributor among the $PM_{2.5}$ chemical species.

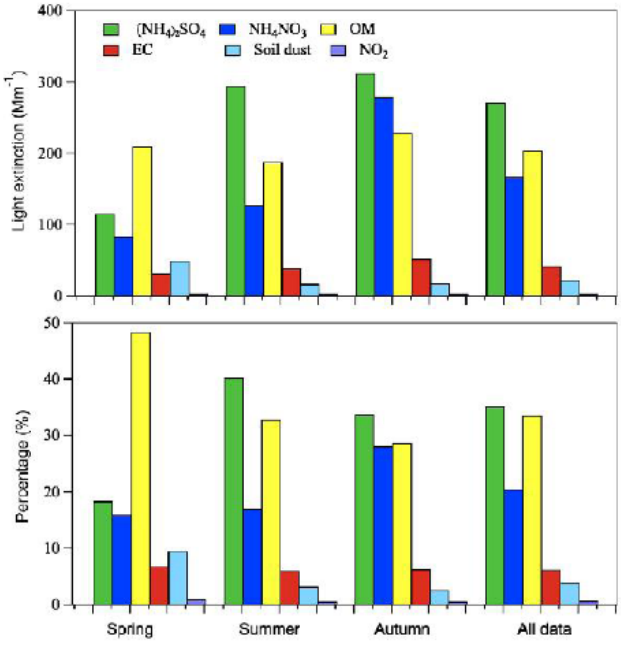

Figure 5: Relative contributions of $PM_{2.5}$ chemical components to light extinction coefficient based on the revised IMPROVE equation during different seasons and entire campaign period.

$(NH_4)_2SO_4$ (116.6 Mm^{-1}) was the second highest contributor to b_{ext}, accounting for 18.4%. The contribution from NH_4NO_3 (84.3 Mm^{-1}) was also large contributing to 16.1% of b_{ext}. The fine soil (50.8 Mm^{-1}) and EC (32.9 Mm^{-1}) contributed minor with 9.5% and 6.9% of b_{ext}. For summer, $(NH_4)_2SO_4$ (295.8 Mm^{-1}) was the largest contributor to b_{ext} accounting for 40.3%, followed by OM (188.5 Mm^{-1}, 32.9%), NH_4NO_3 (128.8 Mm^{-1}, 17.1%), EC (39.5 Mm^{-1}, 6.1%), fine soil (17.8 Mm^{-1}, 3.3%), and NO_2 (3.7 Mm^{-1}, 0.7%). For autumn, $(NH_4)_2SO_4$ (312.7 Mm^{-1}) was still the dominant contributor to b_{ext} contributing 35.3%. The b_{ext} caused by NH_4NO_3 and OM were also abundant which were 279.7 Mm^{-1} and 229.1 Mm^{-1}, accounting for 28.7% and 28.2%, respectively. The EC (52.5 Mm^{-1}), fine soil (18.7 Mm^{-1}), and NO_2 (4.2 Mm^{-1}) contributed minor with 6.4%, 2.6%, and 0.7% of b_{ext}, respectively.

To further investigate the impacts of chemical species on b_{ext} under different $PM_{2.5}$ loadings, we divided the campaign period into polluted period (> 75 μg m^{-3}) and unpolluted period (< 75 μg m^{-3}) based on the Grade II of NAAQS. Figure **6** shows the comparison result of the reconstructed and measured b_{ext} during polluted and unpolluted periods. The reconstructed b_{ext} correlated well with the measured values with the correlation coefficients of 0.90 and 0.93 for polluted and unpolluted periods, respectively, indicating a good consistency between them.

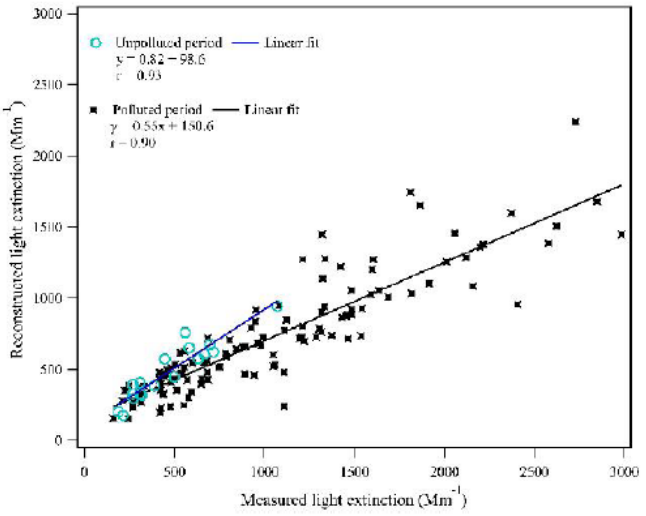

Figure 6: Scatter plot of reconstructed light extinction versus measured one during polluted and unpolluted periods.

Figure **7** shows the contributions of $PM_{2.5}$ chemical composition to b_{ext} during polluted and unpolluted periods. The b_{ext} contributed by chemical composition exhibited the order of $(NH_4)_2SO_4$ > OM > NH_4NO_3 > EC > fine soil > NO_2. The b_{ext} produced by $(NH_4)_2SO_4$, OM, and NH_4NO_3 were 2.5, 1.8, and 2.4 times higher during polluted period compared with the unpolluted period. From the percentage of each chemical species to b_{ext}, the contribution varied slightly, for example, $(NH_4)_2SO_4$ increased from 32.5% on unpolluted period to 36.2% on polluted period; OM decreased from 37.3% on unpolluted period to 32.4% on polluted period; and NH_4NO_3 decreased from 21.0% on unpolluted period to 20.4% on polluted period. Those results indicated that $(NH_4)_2SO_4$ was the most important chemical composition in $PM_{2.5}$ affecting the aerosol optical properties during the XA-IHE period.

4. CONCLUSIONS

An intensive measurement campaign was conducted during Xi'an International Horticultural Expo of China to investigate the impacts of $PM_{2.5}$ chemical composition on aerosol light extinction. The daily $PM_{2.5}$ mass concentration ranged from 23.0 – 318.9 μg m^{-3} with an average value of 118.1 ± 57.3 μg m^{-3} during the entire campaign, which was 1.6 times higher than the Grade II of Chinese National Ambient Air Quality Standards (NAAQS) of daily mass concentration of $PM_{2.5}$ (75 μg m^{-3}). Among the $PM_{2.5}$ chemical species, carbonaceous aerosols (*i.e.*, organic carbon and element carbon) contributed to 23.1% of $PM_{2.5}$ mass while water-soluble inorganic ions accounted for 40.7% of $PM_{2.5}$ mass. For the elements, S, Ca, Zn, K, Cl, and Fe were abundant, which together accounted for 80% of total elements.

The average light extinction was 957.7 ± 643.5 Mm^{-1} with >90% contributed by the light scattering. The light extinction during polluted period was 1.6 times larger than that during unpolluted period. Both light scattering and absorption coefficients showed larger values for polluted period compared with the unpolluted period. The diurnal variations of the measured dry light scattering showed different patterns during different seasons, which was related to the anthropogenic activity pattern of daily life and the daily variation in boundary-layer height. Based on the IMPROVE equation, $(NH_4)_2SO_4$ was the largest contributor to light extinction accounting for 35.3%, followed by organic

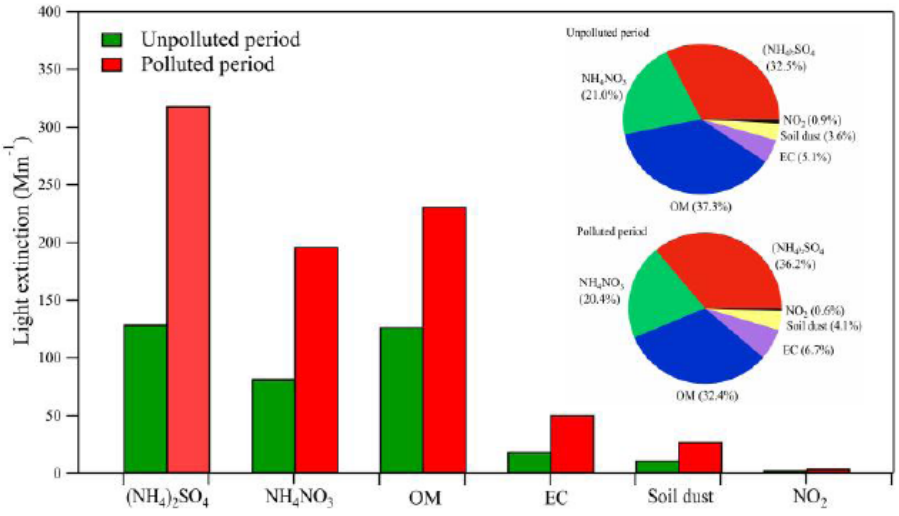

Figure 7: Relative contributions of $PM_{2.5}$ chemical components to light extinction coefficient during polluted and unpolluted periods.

matter (33.7%), NH_4NO_3 (20.5%), EC (6.3%), and fine soil (4.0%). The light extinction produced by $(NH_4)_2SO_4$, organic matter, and NH_4NO_3 were 2.5, 1.8, and 2.4 times higher during polluted period compared with the unpolluted period. The results indicated that $(NH_4)_2SO_4$ was the most important chemical composition in $PM_{2.5}$ affecting the aerosol optical properties during the Xi'an International Horticultural Expo.

ACKNOWLEDGEMENTS

This work was supported by the Key Research and Development Program of Shaanxi Province (2018-ZDXM3-01).

REFERENCE

[1] Li Z, Lau WKM, Ramanathan V, Wu G, Ding Y, Manoj MG, Liu J et al. Aerosol and monsoon climate interactions over Asia. Reviews of Geophysics 2016; 54(4): 866-929. https://doi.org/10.1002/2015RG000500

[2] Samset BH, Sand M, Smith CJ, Bauer SE, Forster PM, Fuglestvedt JS, Osprey S, Schleussner CF. Climate impacts from a removal of anthropogenic aerosol emissions. Geophysical Research Letters 2018; 45(2): 1020-1029. https://doi.org/10.1002/2017GL076079

[3] Shrivastava M, Cappa CD, Fan J, Goldstein AH, Guenther AB, Jimenez JL, Kuang C et al. Recent advances in understanding secondary organic aerosol: Implications for global climate forcing. Reviews of Geophysics 2017; 55(2): 509-559. https://doi.org/10.1002/2016RG000540

[4] Paasonen P, Asmi A, Petaja T, Kajos MK, Aijala M, Junninen H, Holst T et al. Warming-induced increase in aerosol number concentration likely to moderate climate change. Nature Geoscience 2013; 6(6): 438-442. https://doi.org/10.1038/ngeo1800

[5] Mahowald N. Aerosol indirect effect on biogeochemical cycles and climate. Science 2011; 334(6057): 794-796. https://doi.org/10.1126/science.1207374

[6] Deng Q, Deng L, Miao Y, Guo X, Li Y. Particle deposition in the human lung: Health implications of particulate matter from different sources. Environmental Research 2019; 169: 237-245. https://doi.org/10.1016/j.envres.2018.11.014

[7] Zou B, You J, Lin Y, Duan X, Zhao X, Fang X, Campen MJ, Li S. Air pollution intervention and life-saving effect in China. ENVIRONMENT INTERNATIONAL 2019, 125, 529-541. https://doi.org/10.1016/j.envint.2018.10.045

[8] Cao JJ, Wang QY, Chow JC, Watson JG, Tie XX, Shen ZX, Wang P, An ZS. Impacts of aerosol compositions on visibility impairment in Xi'an, China. Atmospheric Environment 2012; 59: 559-566. https://doi.org/10.1016/j.atmosenv.2012.05.036

[9] Fan J, Rosenfeld D, Zhang Y, Giangrande SE, Li Z, Machado LAT, Martin ST et al. Substantial convection and precipitation enhancements by ultrafine aerosol particles. Science 2018; 359(6374): 411-418. https://doi.org/10.1126/science.aan8461

[10] Li J, Chen H, Li Z, Wang P, Fan X, He W, Zhang J. Analysis of low-level temperature inversions and their effects on aerosols in the lower atmosphere. Advances in Atmospheric Sciences 2019; 36(11): 1235-1250. https://doi.org/10.1007/s00376-019-9018-9

[11] Rosenfeld D, Andreae MO, Asmi A, Chin M, de Leeuw G, Donovan DP, Kahn R, et al. Global observations of aerosol-cloud-precipitation-climate interactions. Reviews of Geophysics 2014; 52(4): 750-808. https://doi.org/10.1002/2013RG000441

[12] Wang Q, Cao J, Tao J, Li N, Su X, Chen LWA, Wang P et al. Long-term trends in visibility and at Chengdu, China. PLoS ONE 2013; 8(7): e68894. https://doi.org/10.1371/journal.pone.0068894

[13] Song C, Wu L, Xie Y, He J, Chen X, Wang T, Lin Y wt al. Air pollution in China: Status and spatiotemporal variations. Environmental Pollution 2017; 227: 334-347. https://doi.org/10.1016/j.envpol.2017.04.075

[14] Zheng B, Tong D, Li M, Liu F, Hong C, Geng G, Li H, Li X, Peng L, Qi J, Yan L, Zhang Y, Zhao H, Zheng Y, He K, Zhang Q. Trends in China's anthropogenic emissions since 2010 as the consequence of clean air actions. Atmospheric Chemistry and Physics 2018; 18(19): 14095-14111. https://doi.org/10.5194/acp-18-14095-2018

[15] Deng J, Zhang Y, Hong Y, Xu L, Chen Y, Du W, Chen J. Optical properties of PM2.5 and the impacts of chemical compositions in the coastal city Xiamen in China. Science of The Total Environment 2016; 557-558: 665-675. https://doi.org/10.1016/j.scitotenv.2016.03.143

[16] Liao W, Zhou J, Zhu S, Xiao A, Li K, Schauer JJ. Characterization of aerosol chemical composition and the reconstruction of light extinction coefficients during winter in Wuhan, China. Chemosphere 2020; 241: 125033-125033. https://doi.org/10.1016/j.chemosphere.2019.125033

[17] Tian J, Wang Q, Han Y, Ye J, Wang P, Pongpiachan S, Ni H, Zhou Y, Wang M, Zhao Y, Cao J. Contributions of aerosol composition and sources to particulate optical properties in a southern coastal city of China. Atmospheric Research 2020; 235, 104744-104744. https://doi.org/10.1016/j.atmosres.2019.104744

[18] Wang H, Shi G, Tian M, Zhang L, Chen Y, Yang F, Cao X. Aerosol optical properties and chemical composition apportionment in Sichuan Basin, China. Science of The Total Environment 2017; 577: 245-257. https://doi.org/10.1016/j.scitotenv.2016.10.173

[19] Wang YH, Liu ZR, Zhang JK, Hu B, Ji DS, Yu YC, Wang YS. Aerosol physicochemical properties and implications for visibility during an intense haze episode during winter in Beijing. Atmospheric Chemistry and Physics 2015; 15(6): 3205-3215. https://doi.org/10.5194/acp-15-3205-2015

[20] Wu D, Zhang F, Ge X, Yang M, Xia J, Liu G, Li F. Chemical and light extinction characteristics of atmospheric aerosols in suburban Nanjing, China. Atmosphere 2017; 8(8): 149. https://doi.org/10.3390/atmos8080149

[21] Yu X, Shen L, Xiao S, Ma J, Lu R, Zhu B, Hu J, Chen K, Zhu J. Chemical and optical properties of atmospheric aerosols during the polluted periods in a megacity in the Yangtze River Delta, China. Aerosol and Air Quality Research 2019; 19(1): 103-117. https://doi.org/10.4209/aaqr.2017.12.0572

[22] Zhou Y, Wang Q, Zhang X, Wang Y, Liu S, Wang M, Tian J et al. Exploring the impact of chemical composition on aerosol light extinction during winter in a heavily polluted urban area of China. Journal of Environmental Management 2019; 247: 766-775. https://doi.org/10.1016/j.jenvman.2019.06.100

[23] Bei N, Zhao L, Xiao B, Meng N, Feng T. Impacts of local circulations on the wintertime air pollution in the Guanzhong Basin, China. Science of The Totoal Environment 2017; 592: 373-390. https://doi.org/10.1016/j.scitotenv.2017.02.151

[24] Feng T, Bei N, Zhao S, Wu J, Li X, Zhang T, Cao J, Zhou W, Li G. Wintertime nitrate formation during haze days in the Guanzhong basin, China: A case study. Environmental

Pollution 2018; 243: 1057-1067.
https://doi.org/10.1016/j.envpol.2018.09.069

[25] Niu X, Cao J, Shen Z, Ho SSH, Tie X, Zhao S, Xu H, Zhang B, Huang R. PM2.5 from the Guanzhong Plain: Chemical composition and implications for emission reductions. Atmospheric Environment 2016; 147: 458-469.
https://doi.org/10.1016/j.atmosenv.2016.10.029

[26] Zhang T, Cao JJ, Tie XX, Shen ZX, Liu SX, Ding H, Han YM, Wang GH, Ho KF, Qiang J, Li WT. Water-soluble ions in atmospheric aerosols measured in Xi'an, China: Seasonal variations and sources. Atmospheric Research 2011; 102(1): 110-119.
https://doi.org/10.1016/j.atmosres.2011.06.014

[27] Chow JC, Watson JG, Robles J, Wang X, Chen LWA, Trimble DL, Kohl SD, Tropp RJ, Fung KK. Quality assurance and quality control for thermal/optical analysis of aerosol samples for organic and elemental carbon. Analytical and Bioanalytical Chemistry 2011; 401(10): 3141-3152.
https://doi.org/10.1007/s00216-011-5103-3

[28] Cao JJ, Lee SC, Ho KF, Zhang XY, Zou SC, Fung K, Chow JC, Watson JG. Characteristics of carbonaceous aerosol in Pearl River Delta Region, China during 2001 winter period. Atmospheric Environment 2003; 37(11): 1451-1460.
https://doi.org/10.1016/S1352-2310(02)01002-6

[29] Watson JG, Chow JC, Frazier CA. X-ray fluorescence analysis ofambient air samples. Elemental Analysis of Particles 1999; 1: 67-96.

[30] Watson JG. Visibility: science and regulation. Journal of the Air & Waste Management Association 2002; 52(6): 628-713.
https://doi.org/10.1080/10473289.2002.10470813

[31] Chen J, Zhao CS, Ma N, Yan P. Aerosol hygroscopicity parameter derived from the light scattering enhancement factor measurements in the North China Plain. Atmospheric Chemistry and Physics 2014; 14(15): 8105-8118.
https://doi.org/10.5194/acp-14-8105-2014

[32] Malm WC, Day DE, Kreidenweis SM, Collett JL, Lee T. Humidity-dependent optical properties of fine particles during the Big Bend Regional Aerosol and Visibility Observational Study. Journal of Geophysical Research: Atmospheres 2003; 108(D9): 4279.
https://doi.org/10.1029/2002JD002998

[33] Laskin A, Laskin J, Nizkorodov SA. Chemistry of atmospheric brown carbon. Chemical Reviews 2015; 115(10): 4335-4382.
https://doi.org/10.1021/cr5006167

[34] Pitchford M, Malm W, Schichtel B, Kumar N, Lowenthal D, Hand J. Revised algorithm for estimating light extinction from IMPROVE particle speciation data. Journal of the Air & Waste Management Association 2007; 57(11): 1326-1336.
https://doi.org/10.3155/1047-3289.57.11.1326

[35] Turpin BJ, Lim HJ. Species contributions to PM2.5 mass concentrations: revisiting common assumptions for estimating organic mass. Aerosol Science and Technology 2001; 35(1): 602-610.
https://doi.org/10.1080/02786820119445

[36] Taylor SR, McLennan SM. The continental crust: Its composition and evolution. Blackwell, Oxford 1985.

Received on 23-12-2019 Accepted on 10-1-2020 Published on 23-1-2020

DOI: https://doi.org/10.12974/2311-8741.2020.08.4